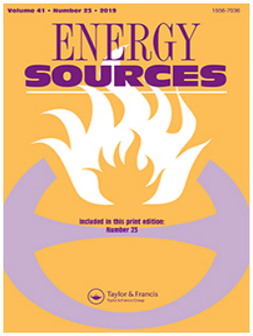

Energy Sources, Part A: Recovery, Utilization, and Environmental Effects

ISSN: 1556-7036 (Print) 1556-7230 (Online) Journal homepage: https://www.tandfonline.com/loi/ueso20

CFD-simulation-based optimization of superheater for steam production from waste heat of SRF combustor

Yunji Kim, Sengryong Park, Chongpyo Cho, Gyuin Yeom & Youngsoon Baek

To cite this article: Yunji Kim, Sengryong Park, Chongpyo Cho, Gyuin Yeom & Youngsoon Baek (2019) CFD-simulation-based optimization of superheater for steam production from waste heat of SRF combustor, Energy Sources, Part A: Recovery, Utilization, and Environmental Effects, 41:23, 2944-2955, DOI: 10.1080/15567036.2019.1643949

To link to this article: https://doi.org/10.1080/15567036.2019.1643949

ENERGY SOURCES, PART A: RECOVERY, UTILIZATION, AND ENVIRONMENTAL EFFECTS
2019, VOL. 41, NO. 23, 2944–2955
https://doi.org/10.1080/15567036.2019.1643949

Taylor & Francis
Taylor & Francis Group

CFD-simulation-based optimization of superheater for steam production from waste heat of SRF combustor

Yunji Kim[a], Sengryong Park[b], Chongpyo Cho[b], Gyuin Yeom[a], and Youngsoon Baek[a]

[a]Department of Environment-Energy, The University of Suwon, Hwaseong, Korea; [b]Korea Institute of Energy Research, Daejeon, Korea

ABSTRACT

A superheater uses waste heat from a combustor or an incinerator to produce superheated steam through heat exchange between saturated steam and exhaust (flue) gas. Superheaters predominantly use thin tube-type pipes, which makes it difficult to experimentally determine internal phenomena such as the flow, pressure distribution, and temperature distribution. Computational fluid dynamics (CFD) has recently been used to successfully analyze superheaters. In this study, steam at 180°C and 3.4 bars was converted via a cylindrical superheater into superheated steam above 700°C and 3bars using exhaust gas at 900°C from a solid refuse fuel combustor. The superheated steam was then supplied to a high-temperature solid oxide electrolyte cell to increase the hydrogen production efficiency of water electrolysis. CFD analyses were also conducted using a commercial Fluent simulator to study the effects of the furnace size, superheater size, inlet and outlet diameters, and steam generation amount on the exit temperature. The CFD simulation results were determined to be valid by a pilot experimental apparatus, which showed that the error rate between the experimental measurements and the simulation results was less than 2%. For the same volume, the superheater with the largest surface area (0.4-m diameter and 1-m length) produced the highest exit temperature. For steam inlet and outlet diameters of 8 mm, the highest exit temperature was 652°C. By reducing the flow rate to 70 kg/h, steam at over 700°C and 3 bars could be obtained under these optimal conditions.

ARTICLE HISTORY
Received 7 February 2019
Revised 5 June 2019
Accepted 30 June 2019

KEYWORDS
Computational fluid dynamics (CFD); superheater; heat exchange; high-temperature steam; radiation; exit temperature

Introduction

In recent years, global goals regarding the climate change mitigation have focused considerable attention on energy generation from renewable sources. Accordingly, the traditional role of the recovery combustors is changing, and the focus is shifting toward simultaneously maximizing the generation of renewable energy. To achieve these goals, it is important to understand the combustion and heat exchange tubes of such combustors and to develop modeling methods to optimize their efficiency (Maakala, Jarvinen, and Vuorinen 2018a). Various types of heat exchange tubes are used in superheaters, evaporators, and economizers. The superheater is typically located at the end of the boiler, and it is exposed to the highest pressure and temperature conditions. Flow properties, such as the size and arrangement of the tubes and the velocity of the working fluid, are important factors to consider when designing superheaters for modern thermal plants (Jones 2004; Lee, Han, and Choi 2018). Because it is difficult to explain the complicated flow and heat phenomena, the superheater temperature is usually predicted experimentally, and rarely through mathematical modeling

CONTACT Youngsoon Baek ysbaek@suwon.ac.kr Department of Environment-Energy, The University of Suwon, 17 Wauan-gil, Bongdam-eup, Hwaseong 18323, Korea

Color versions of one or more of the figures in the article can be found online at www.tandfonline.com/ueso.

(Chaibakhsh, Ghaffari, and Moosavian 2007; Ghaffari, Chaibakhsh, and Parsa 2007). Recently, efforts have been made to analyze superheaters through computational fluid dynamics (CFD) (Drosatos et al. 2014; Jukola, Kyttälä, and McKeough 2014; Mueller et al. 2014; Park et al. 2010; Salcudean, Nowak, and Abdullah 1993; Schuhbauer et al. 2014; Vakkilainen et al. 1998). Lundborg analyzed a superheater using 2D and 3D shapes to obtain high-temperature steam by increasing the heat exchange efficiency of the superheater, found improvements in the flow and heat transfer of the flue gas (i.e., heat source), and simulated the internal flow according to the recirculation method of the superheater (Lundborg 2005). A superheater that can perform high-temperature heat exchange has higher energy production efficiency than a conventional heat exchanger because it converts steam into a superheated state at a temperature higher than that of the saturation state through heat exchange between the steam and the flue gas (Shin and Lee 2010). The superheater produces superheated steam through the heat exchange between the steam flowing through circular pipes such as tubes and the flue gas that flows over these pipes.

From a thermodynamics point of view, a portion of the energy required for endothermic water splitting can be obtained from high-temperature heat from excess heat from combustor flue gas, hence significantly reducing the electric energy demand. Furthermore, high-temperature electrolysis not only splits water molecules but also those of carbon dioxide or a mixture of both to produce synthesis gas or other energy carriers such as methane or methanol by subsequent catalytic conversion (Ebbesen et al. 2014; Foit et al. 2017; Kondratenko et al. 2013). If the water can be converted into steam by waste heat from other processes it is more efficient for high-temperature electrolysis (HTE) to convert steam directly. The reasons are the more favorable thermodynamic and electrochemical kinetic conditions for the reaction. Thermodynamic conditions are more favorable in that the molar Gibbs energy of the reaction (ΔG) drops from ~1.23 eV (237 kJ/mol) at ambient temperature to ~0.95 eV at 900°C (183 kJ/mol), while the molar enthalpy of the reaction (ΔH) remains essentially unchanged (ΔH ~1.3 eV or 249 kJ/mol at 900°C). A significant part of the energy required for an ideal (loss-free) HTE can thus be provided by heat ($T\Delta S$) coming from external sources or due to the unavoidable Joule effect in the electrolyzer cell. As a consequence, less electricity is required per m^3 of H_2 generated compared with the other electrolyzer technologies as shown in Figure 1. The transfer from water to steam electrolysis significantly reduces the electricity demand, followed by a continuous decrease with increasing temperature. The theoretical SOEC

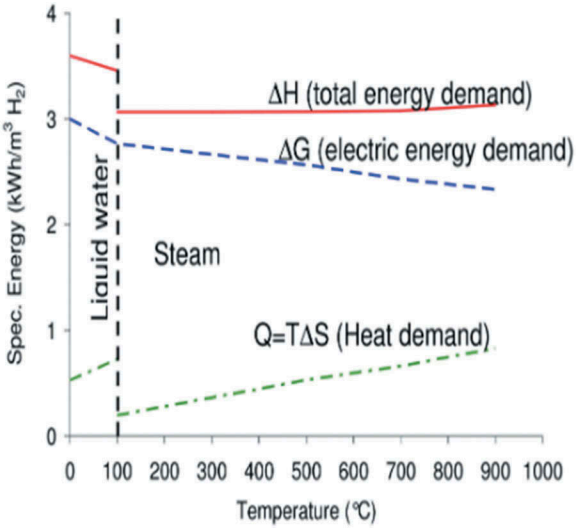

Figure 1. Energy demand of hydrogen operation versus operation temperature(Doenitz et al. 1980).

electrical efficiency is close to 100% for a hydrogen production efficiency of 90% (Schiller, Lang, and Sundarraj 2019).

In the present study, steam at over 180°C and 3.4 bars generated from a boiler were converted using a cylindrical steam superheater into superheated steam at over 700°C and 3 bars using the waste heat of the exhaust gas at 900°C from a solid refuse fuel (SRF) combustor. Superheated steam at over 700°C was then supplied to a high-temperature solid oxide electrolyte cell to increase the hydrogen production efficiency of water electrolysis. CFD analysis was conducted on the effects of furnace and superheater size, superheater inlet and outlet diameters, and the steam generation amount of the cylindrical steam superheater on the exit temperature using a commercial Fluent simulator to determine the optimal conditions to produce steam at over 700°C under the above-mentioned furnace conditions.

Experimentation and simulation of superheater in SRF combustion process

Figure 2 shows the cylindrical SRF combustor (length: 2.065 m, diameter: 1.28 m) used in the present study as the heat source of the superheater. The combustion of SRF fuel (low heating value ≒ 4,557 kcal/kg) at a rate of 50 kg/h with an air ratio of 1.86 generates exhaust gas with a temperature of approximately 900°C. This exhaust gas was introduced to the second furnace (length: 1.7 m, diameter: 0.97 m) through a 0.1-m-diameter pipe and exhausted after heat exchange with the steam inside the superheater located at the center of the furnace. Steam at a temperature of 180°C and pressure of 3.4 bars was introduced into the superheater at a rate of 100 kg/h. The superheater produces high-temperature superheated steam by increasing the heat exchange area by using circular coil- or tube-type pipes (Maakala, Jarvinen, and Vuorinen 2018b). Both types of pipes increase the heat exchange efficiency according to their length; however, if they contain deposits such as ash or have suffered corrosion damage, they may also degrade the local heat exchange efficiency (Lorente et al. 2013; Weber et al. 2013). Furthermore, both types of pipes suffer a pressure drop at their outlets. Therefore, a cylindrical superheater was used in this study to improve the pressure drop constraints and to obtain high-temperature steam.

The Ansys Fluent v18.2 commercial code was used for the CFD analysis. Heat transfer between high-temperature exhaust gas and steam was analyzed using the Navier–Stokes equations and energy equations. In this instance, the equations governing the mass, momentum, and energy required for the analysis of fluid and energy movement phenomena can be expressed as follows:

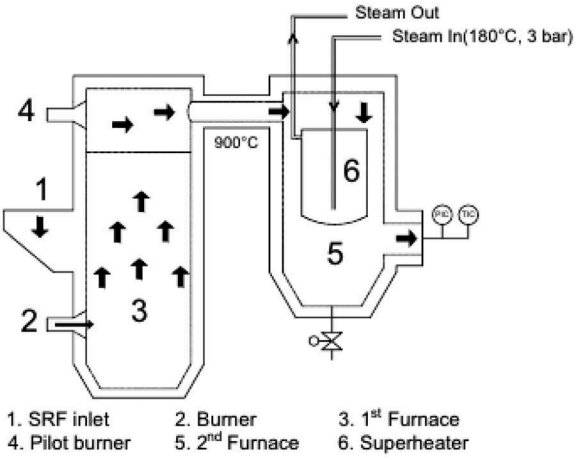

Figure 2. Schematic of SRF furnace, second furnace, and superheater.

$$\text{Mass conservation equation}: \frac{\partial \mathrm{p}}{\partial \mathrm{t}} + \nabla \cdot (\rho \vec{\mathrm{v}}) = \mathrm{S_m} \tag{1}$$

$$\text{Momentumconservation equation}: \frac{\partial}{\partial \mathrm{t}}(\mathrm{p}\vec{\mathrm{v}}) + \nabla \cdot (\rho \vec{\mathrm{v}}\vec{\mathrm{v}}) = -\nabla \mathrm{p} + \nabla \cdot (\bar{\tau}) + \rho \vec{\mathrm{g}} + \vec{\mathrm{F}} \tag{2}$$

$$\text{Energyconservation equation}: \frac{\partial(\rho h)}{\partial t} - \frac{\partial p}{\partial t} + \nabla\left(\rho \vec{v} h\right) = \nabla(\lambda \nabla h) + \vec{v}\nabla p + \tau : \nabla v + S_E \tag{3}$$

where u_i is the velocity (m/s); P, the pressure (Pa); ρ, the density (kg/m^3); t, the time (s); k, the conductivity (W/m·K); and C_p, the specific capacity (j/kg·K).

To calculate the flow from the fast-flowing exhaust gas in the furnace and the steam inside the superheater, the standard k-ε turbulence model was used. Radiation from the furnace walls must also be considered for exhaust gas at 900°C. Therefore, Discrete Ordinates (DO), a widely applicable radiation model in Fluent, was used.

To simulate the shape and conditions of the superheater that produces superheated steam at over 700°C and 3.4 bars from steam at approximately 180°C and 3.4 bars, modeling was performed, as shown in Figure 1. The simulation was performed for a superheater with 0.66-m length and 0.5-m diameter (volume ≒ 0.13 m^3) installed at the center inside the second furnace. In the simulation, the steady-state analysis was conducted.

Experimental equipment

To conduct experiments for the superheater, the cylindrical Pilot combustor presented in Table 1 was manufactured with the length and diameter of 1.6 m and 1 m, respectively. The exhaust gas flows into the bottom inlet of the combustor and flows out of its top outlet. In the combustor, 8.5 Nm^3/hr of natural gas is combusted with excess air at a ratio of 1.2, and exhaust gas is generated at approximately 124 kg/hr. Furthermore, as shown in Figure 3, the experimental superheater has a diameter of 0.2 m, length of 0.4 m, and head of 0.097 m. The heat is exchanged at a steam flow rate of 15 kg/hr and a pressure of 4 bar. Figure 4 shows the dimensions of second furnace and superheater with inlets and outlets.

Table 1. Condition of flue gas and steam.

Flue gas		Steam		
Flow rate (kg/hr)	Temperature (°C)	Flow rate (kg/hr)	Temperature (°C)	Pressure (bar)
124	950	15	145	4

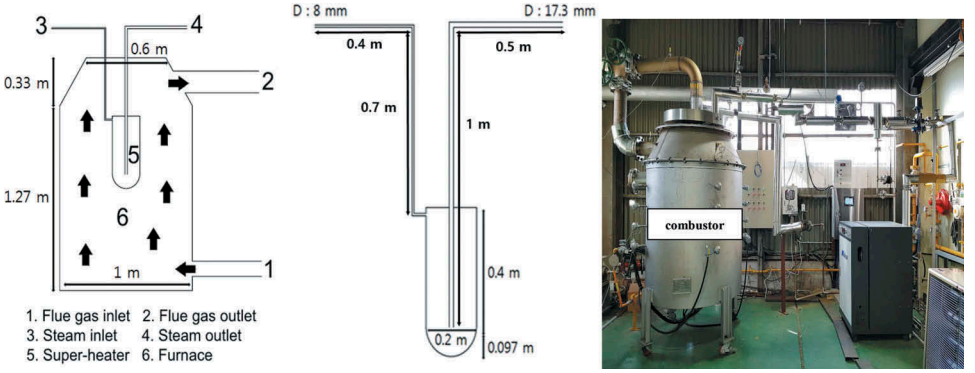

Figure 3. Experimental Pilot Combustor & Superheater.

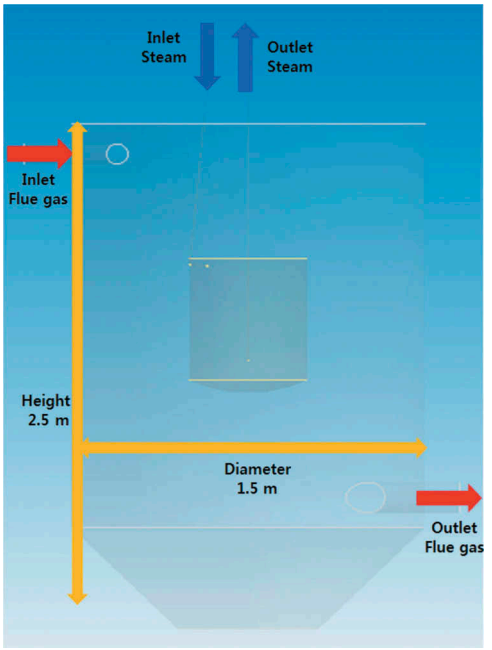

Figure 4. Dimensions of second furnace and superheater with inlets and outlets.

Model equation and simulation condition

The outer wall of the steam superheater was made of 5-mm-thick SUS310 steel. Table 2 lists the flow rates, temperatures, and pressures of the exhaust gas and steam. Figure 5 shows the shape and specifications of the superheater for the simulation.

Case study conditions for simulation

As mentioned above, in the simulation, the length and diameter of the superheater were varied over the values listed in Table 3 to identify the exit temperature according to the surface area of the superheaters for the same (0.13 m^3) or different volumes inside the furnace.

To identify the effects of different configurations of the superheater, the first simulation was performed for incidence angles of 0°, 1°, and 5°, as shown in Table 4, because the incidence angle of steam appears to affect the residence time in the superheater and the amount of heat transfer. To identify the effects of different diameters of the pipe inlet and outlet of the superheater on exit temperature, a second simulation was performed with the inlet diameter fixed at 8 or 30 mm and the outlet diameter varied as 8, 15, and 30 mm, as shown in Table 4. Finally, the exhaust gas was directly injected onto the superheater, and the exit temperature was compared with that under the previous tangential flow. Figure 6 shows the configurations of the superheater.

Table 2. Parameter values at the inlets and outlets of the furnace and superheater.

Parameter	Flue gas	Steam
Flow rate (kg/h)	667	100
Temperature (K)	1173.15	453.15
Pressure (bar)	1.0	3.4

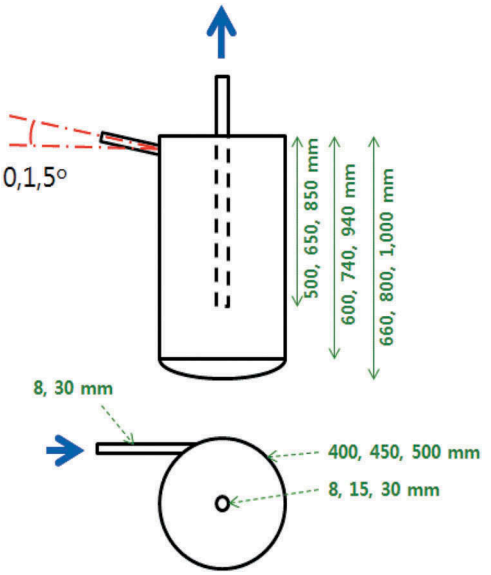

Figure 5. Dimensions and specifications of the superheater.

Table 3. Dimensions of furnace and superheater.

		Superheater				
Furnace (D × L m)		Length (m)	Diameter (m)	Surface area (m^2)	Volume (m^3)	Other
(1)	1.5 × 2.5	0.66	0.5	1.429	0.13	reference
		0.80	0.45	1.448		
		1	0.4	1.5072		
(2)	0.97 × 1.7	1	0.4	1.5072	0.13	
		1	0.45	1.7308	0.16	
		1	0.5	1.9625	0.20	

Table 4. Experimental conditions for different configurations of superheater.

Condition		Case 1	Case 2	Case 3
Incidence angle (°)		0	1	5
Pipe diameter (mm)			Outlet	
Inlet	8	8	15	30
	30			
Flow type of exhaust gas		tangential	orthogonal	-

To simulate their effects on exit temperature, the length and diameter of the second furnace were reduced from 2.5 m and 1.5 m to 1.7 m and 0.97 m, respectively, and the diameter of the superheater was varied as 0.4, 0.45, and 0.5 m, as shown in Table 5. In particular, the size of the superheater was increased to up to one-half the size of the second furnace to avoid affecting the exhaust gas flow, and the diameter was varied as 0.4, 0.45, and 0.5 m. The flow rate of the steam was changed from 70 to 100 kg/h under optimal conditions to determine its effects on the temperature and pressure at the steam outlet.

Results and discussion

Experimental verification

Experiments were conducted using the experimental apparatus presented in Figure 3 and the experimental conditions listed in Table 2. The effectiveness of superheater was found to be approximately 0.7, and the steam outlet temperature of the superheater was found to be

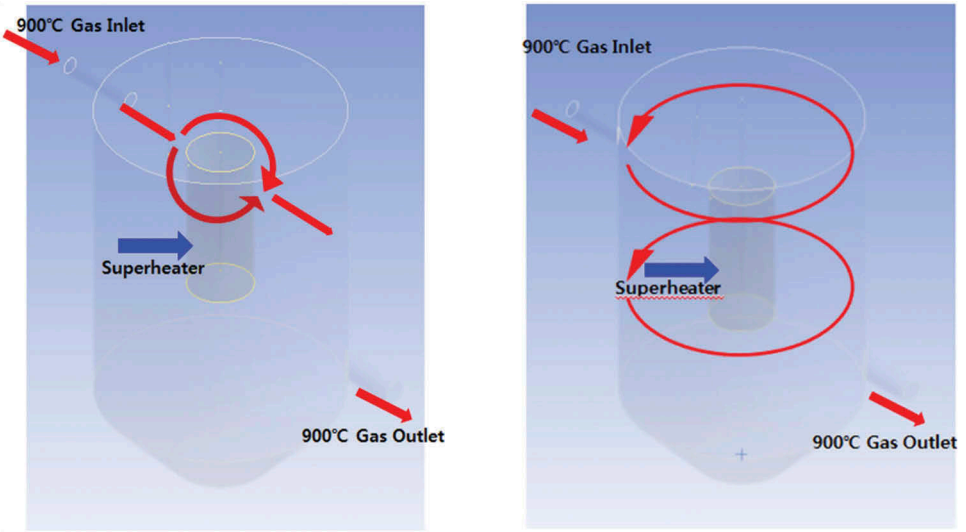

Figure 6. Tangential and orthogonal flows of exhaust gas against superheater wall.

Table 5. Experimental conditions for superheater configurations.

Condition	Length (m)	Diameter (m)	Surface area (m^2)
Case 1	1	0.4	1.5072
Case 2		0.45	1.7308
Case 3		0.5	1.9625

approximately 701°C. The outlet temperature of the superheater in the CFD analysis was found to be approximately 708°C, and the flow pattern and the temperature contour are shown in Figures 7 and 8, respectively. As shown in Figure 7, the exhaust gas in the combustor shows rotational flow. Further, from the temperature contour analysis in Figure 8, it was found that the combustor and the superheater have virtually uniform temperature through active heat transfer. The simulation results agreed well with the experimental measurements; this validates the simulation data.

Effect of the surface area of superheater on exit temperature

Table 6 shows the exit temperature of superheaters with different surface areas installed in furnaces of the same size. For both furnace sizes, the exit temperature of the superheater increased with its surface area. This is a typical trend because heat transfer was proportional to the surface area and a large amount of heat was transferred to the superheater (Schiller, Lang, and Sundarraj 2019). In particular, when the surface was increased by 0.0782 m^2 compared with the reference shape, the exit temperature increased from approximately 15°C to 655°C.

Figure 9 shows the temperature distribution inside the superheater as determined through CFD simulations. The temperature distribution inside the superheater was higher and more uniform, whereas that inside the furnace decreased as the surface area increased, indicating that relatively more heat was transferred to the superheater.

As the diameter of the superheater increased, its surface area and, in turn, area for heat exchange increased, and therefore, the exit temperature increased. When the diameter increased from 0.4 to 0.5 m, the surface area increased by approximately 0.45 m^2 and the exit temperature increased from 13°C to 652°C.

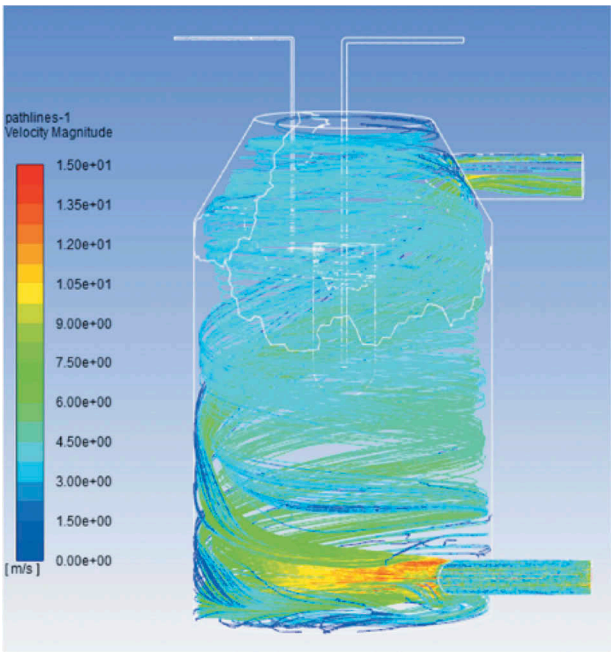

Figure 7. Flow pattern of exhaust gas over Combustor.

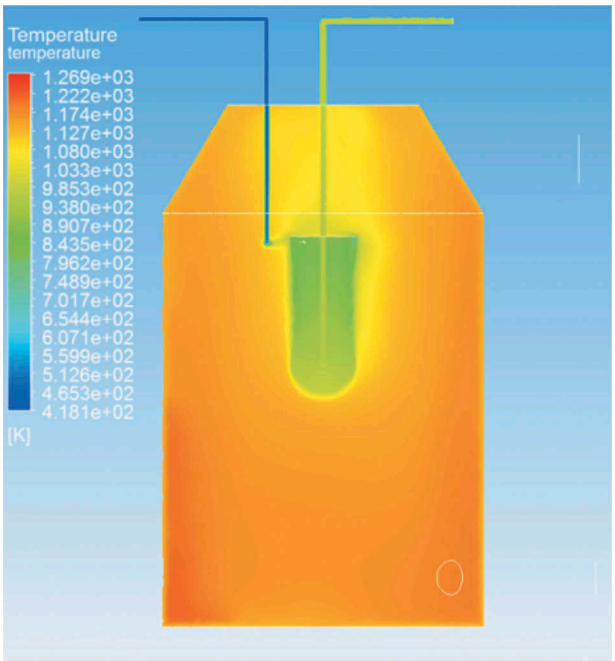

Figure 8. Temperature contour over Combustor.

Effect of superheater shape on exit temperature

Tables 7–9, respectively, show simulation results for the effects of the incidence angle, pipe size, and exhaust gas flow on the exit temperature. Table 7 shows that when the incidence angle was

Table 6. Exit temperature according to sizes of furnace and superheater.

Furnace size (D × L m)		Length (m)	Diameter(m)	Surface area (m^2)	Exit temperature (□)	Other
(1)	1.5 × 2.5	0.66	0.5	1.429	640	reference
		0.88	0.45	1.448	645	
		1	0.4	1.5072	655	
(2)	0.97 × 1.7	1	0.4	1.5072	639	reference
		1	0.45	1.7308	647	
		1	0.5	1.9625	652	

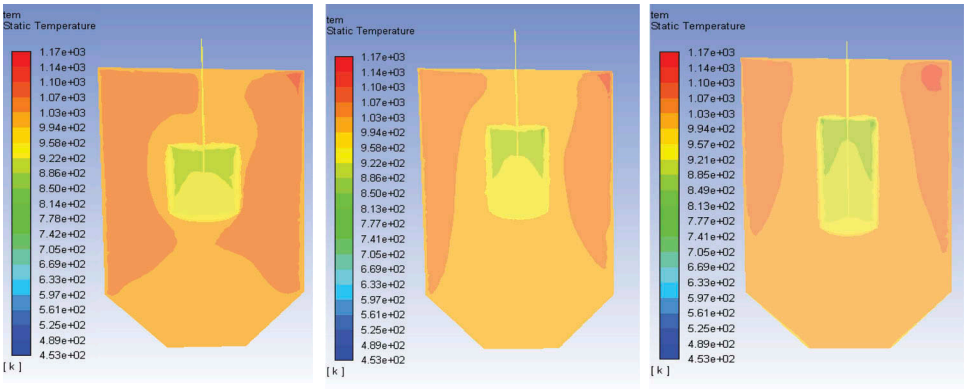

Figure 9. Internal temperature distribution according to superheater size.

Table 7. Effect of incidence angle on exit temperature of steam.

Incidence angle (°)	Exit temperature (□)
0	655.0
1	653.4
5	655.1

Table 8. Effects of inlet and outlet pipe diameters on exit temperature of steam.

	Outlet pipe diameter (mm)					
	8		15		30	
Inlet pipe diameter (mm)	Temperature (°C)	Pressure (bar)	Temperature (°C)	Pressure (bar)	Temperature (°C)	Pressure (bar)
8	655	6.8	657	0.4	655	0.04
30	628	6.8	634	0.4	635	0.19

Table 9. Effect of exhaust gas flow on exit temperature of steam.

Exhaust gas flow	Exit temperature (°C)
Tangential flow	655
Orthogonal flow	650

varied as 0°, 1°, and 5°, the exit temperature varied as 655.1°C, 653.4°C, and 655.0°C, respectively, indicating that the tangential angle did not significantly affect the exit temperature. Therefore, the incidence angle of steam does not seem to significantly affect the exit temperature. The pressure inside the superheater was approximately 6.8 bars.

Table 8 shows that when the outlet diameter was varied as 8, 15, and 30 mm with a pipe inlet diameter of 8 mm, the exit temperature varied only slightly as 655°C, 657°C, and 655°C, respectively, whereas the pressure decreased. As the pressure inside the superheater must be higher than 3 bars, outlet diameters of 15 and 30 mm are inappropriate because the pressure is approximately 0.4 bars or less in these cases. Therefore, pipe inlet and outlet diameters of 8 mm that produced the temperature of 655°C and pressure of 6.8 bars appear to be the optimal conditions.

From Table 9, it can be seen that when the exhaust gas was directly injected onto the superheater, the exit temperature was approximately 650°C; this was approximately 5°C lower than that in the case of a tangential flow. This may be because directly injected air is scattered in all directions and emitted through the outlet after making contact with the superheater, resulting in less heat transfer than in the case of a tangential flow surrounding the superheater, as shown in Figure 10.

Effect of furnace size on exit temperature

Two furnace sizes were simulated to determine their effect on exit temperature for the same superheater size; the results are summarized in Table 10. As the furnace size decreased, heat transfer to the superheater decreased and therefore the exit temperature decreased from 16°C to 639°C.

Effect of a flow rate change on exit temperature

Table 11 shows the exit temperature when the flow rate was varied from 70 to 100 kg/h in increments of 5 kg/h. In this case, the second furnace has 1.7-m length and 0.97-m diameter. The

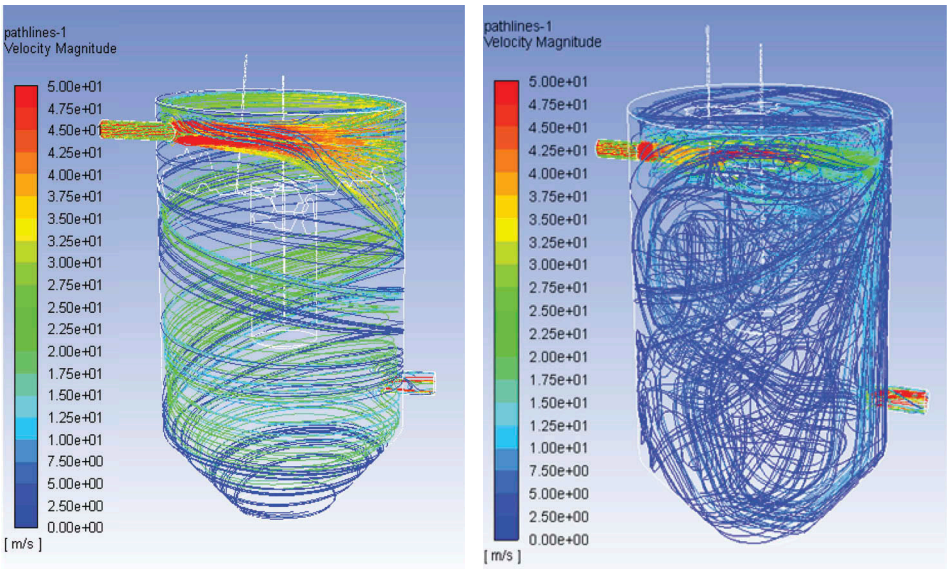

Figure 10. Flow pattern of exhaust gas over combustor.

Table 10. Effect of furnace size on exit temperature of steam.

Furnace size (D × L m)	Length (m)	Diameter (m)	Surface area (m^2)	Exit temperature (□)	Other
1.5 × 2.5	1	0.4	1.5072	655	reference
0.97 × 1.7	1	0.4	1.5072	639	

Table 11. Effect of flow rate on exit temperature of steam.

Flow rate (kg/h)	70	75	80	85	90	95	100
Exit temperature (□)	709	699	689	679	669	661	652

exit temperature decreased as the flow rate increased. In particular, for flow rate of 70 kg/h, the exit temperature was approximately 709°C and pressure was 3.0 bars; for flow rate of 75 kg/h, the corresponding values were 699°C and 3.4 bars. Therefore, for flow rate of 70–75 kg/h, steam at approximately 700°C and 3.4 bars was obtained.

Conclusion

CFD simulations with various variables were conducted for a reference superheater with 0.5-m diameter and 0.66-m length (surface area ≒ 1.429 m^2) that produced superheated steam with an exit temperature of 900°C from steam with a temperature of 180°C and pressure of 3.4 bars flowing at a rate of 100 kg/h. The following results were obtained in this study.

(1) The steam outlet temperature of the superheater was found to be approximately 701°C in the experiment, and the steam outlet temperature of the superheater in the CFD analysis was found to be approximately 708°C under the same experimental conditions. Thus, the simulation data were considered valid because the error rate between the experimental measurements and simulation results was less than 2%.
(2) For superheaters with the same volume, as their surface area was increased to 1.429, 1.448, and 1.5072 m^2, the exit temperature of steam increased to 640, 645, and 655°C, respectively. For surface area of 1.5072 m^2 (0.4-m diameter and 1-m length), the highest exit temperature of 655°C was obtained; this was approximately 15°C higher than that obtained with the reference superheater (surface area of 1.429 m^2). These results indicate that a superheater with larger surface area provides better heat exchange for the same volume.
(3) Simulations showed that when the exhaust gas was directly injected onto the superheater, the exit temperature of steam was 650°C; by contrast, for a tangential flow surrounding the superheater, the exit temperature was 655°C. Therefore, the tangential flow is produced at approximately 5°C higher exit temperature than the orthogonal flow over the superheater.
(4) When the steam incidence angle of the superheater was varied as 0°, 1°, and 5°, the exit temperature was 655, 653, and 655°C, respectively. The temperature varied within approximately 2°C, indicating that it was not significantly affected by the tangential angle. The pressure remained at 6.8 bars.
(5) When the outlet diameter was varied as 8, 15, and 30 mm with an inlet diameter of 8 mm, the exit temperature was 655, 657, and 655°C, respectively. When the outlet diameter was similarly varied with inlet diameter of 30 mm, the exit temperature was 628, 634, and 635°C, respectively. For inlet diameter of 8 mm, the exit temperature was up to 27°C higher than when the inlet diameter was 30 mm. The inlet and outlet diameters of 8 mm provided the best exit temperature and pressure.
(6) The highest exit temperature was obtained for a superheater with 0.5-m diameter and 1-m length installed inside a second furnace with 0.97-m diameter and 1.7-m length with steam inlet and outlet diameters of 8 mm, steam incidence angle of 5°, and tangential flow of the exhaust gas. When the flow rate was decreased from 100 to 70 kg/h in steps of 5 kg/h under these conditions, the steam exit temperature increased by approximately 9–10°C with each decrease. The highest exit temperature of 709°C was obtained for steam flow rate of 70 kg/h; the pressure was approximately 3 bars.

Acknowledgments

This subject is supported by the "Technologies for Waste Recycling Policy" funded by the Korea Ministry of Environment (MOE) as the "Public Technology Program based on Environmental Policy" (2016000710007).

References

Chaibakhsh, A., A. Ghaffari, and S. A. A. Moosavian. 2007. "A simulated model for a once-through boiler by parameter adjustment based on genetic algorithms". *Simulation Modelling Practice and Theory* 15 (9):1029–51. doi:10.1016/j.simpat.2007.06.004.

Doenitz, W., R. Schmidberger, E. Steinheil, and R. Streicher. 1980. Hydrogen production by high temperature electrolysis of water vapour, Int. *International Journal of Hydrogen Energy* 5 (1):55–63. doi:10.1016/0360-3199(80)90114-7.

Drosatos, P., N. Nikolopoulos, M. Agraniotis, G. Itskos, P. Grammelis, and E. Kakaras. 2014. Decoupled CFD simulation of furnace and heat exchangers in a lignite utility boiler. *Fuel* 117:633–48. doi:10.1016/j.fuel.2013.09.033.

Ebbesen, S. D., S. H. Jensen, A. Hauch, and M. B. Mogensen. 2014. High temperature electrolysis in alkaline, solid proton conducting cells, and solid oxide cells. *Chemical Review* 114:10697–734.

Foit, S. R., L. Dittrich, V. Vibhu, I. C. Vinke, R. A. Eichel, and L. G. J. de Haart. 2017. Co-electrolysis, quo vadis? *ECS Transactions*78:3139–47.

Ghaffari, A., A. Chaibakhsh, and H. Parsa, An optimization approach based on genetic algorithm for modeling benson type boiler, American Control Conference, New York, NY, 2, 4860–65,2007.

Jones, D. R. H. 2004. Creep failures of overheated boiler, superheater and reformer tubes. *Engineering Failure Analysis* 11:873–93. doi:10.1016/j.engfailanal.2004.03.001.

Jukola, P., J. Kyttälä, and P. McKeough. 2014. Predicting sodium release in recovery boilers in conjunction with CFD furnace modelling. *Journal of Science & Technology for Forest Products and Processes* 4 (4):48–55.

Kondratenko, V., G. Mul, J. Baltrusaits, G. O. Larrazabal, and J. P. Perez-Ramirez. 2013. Status and perspectives of CO2 conversion into fuels and chemicals by catalytic, photocatalytic and electrocatalytic processes. *Energy & environmental science Science* 6:3112–35.

Lee, Y., S. Han, and S. K. Choi. 2018. Multidisciplinary materials and geometry optimization of superheater tubes for advanced ultra-supercritical power boilers. *Journal of Mechanical Science and Technology* 32 (7):3359–69. doi:10.1007/s12206-018-0639-1.

Lorente, S., J. Lee, Y. Kim, and A. Bejan December 2013. Power from a hot gas stream with multiple superheaters and reheaters. *International Journal of Heat and Mass Transfer* 67:153–58. doi: 10.1016/j.ijheatmasstransfer.2013.07.048.

Lundborg, A. 2005. *Simulation of the flow through the superheater in a recovery boiler*. Stockholm, Sweden: KTH-Royal Institute of Technology.

Maakala, V., M. Jarvinen, and V. Vuorinen. 2018a. Computationalfluid dynamics modeling and experimental validation of heattransfer andfluidflow in the recovery boiler superheater region. *Applied Thermal Engineering* 139:222–38. doi:10.1016/j.applthermaleng.2018.04.084.

Maakala, V., M. Jarvinen, and V. Vuorinen. October 1 2018b. Optimizing the heat transfer performance of the recovery boiler superheaters using simulated annealing, surrogate modeling, and computational fluid dynamics. *Energy* 160: 361–77. doi:10.1016/j.energy.2018.07.002.

Mueller, C., K. Eklund, M. Forssen, and M. Hupa. 2014. Influence of liquor-to-liquor differences on recovery furnace processes - a CFD study. *Proceedings: International Chemical Recovery Conference* 2:979–97.

Park, H. Y., M. Faulkner, M. D. Turrell, P. J. Stopford, and D. S. Kang. 2010. Coupled fluid dynamics and whole plant simulation of coal combustion in a tangentially-fired boiler. *Fuel* 89:2001–10. doi:10.1016/j.fuel.2010.01.036.

Salcudean, M., P. Nowak, and Z. Abdullah. 1993. Cold flow computational model of a recovery boiler. *Journal of pulp and paper science* 19 (5):186–94.

Schiller, G., M. Lang, and P. Sundarraj. 2019. Solar heat intengrated solid oxide steam electrolysis for highly efficient hydrogen production. *Journal of Power Sources* 416:72–78. doi:10.1016/j.jpowsour.2019.01.059.

Schuhbauer, C., M. Angerer, H. Spliethoff, F. Kluger, and H. Tschaffon. 2014. Coupled simulation of a tangentially hard coal fired 700°C boiler. *Fuel* 122:149–63. doi:10.1016/j.fuel.2014.01.032.

Shin, H. B., and S. Y. Lee. 2010. Temperature control of superheater steam in thermal power plant. *The Ttransactions of the Korean Institute of Electrical Engineers* 59 (11): 2006–2011.

Vakkilainen, E. K., L. Kjäldman, V. Taivassalo, P. Kilpinen, and T. Norström. 1998. High solids firing in an operating recovery boiler - comparison of CFD predictions to practical observations in the furnace. *Proceedings: International Chemical Recovery Conference* 1:245–56.

Weber, R., M. Mancini, N. S. Mancini, and T. Kupka. 2013. On predicting the ash behaviour using computational fluid dynamics. *Fuel Processing Technology* ISSN: 0378–3820. 105:113–28. doi:10.1016/j.fuproc.2011.09.008.